RSC Advances

PAPER

View Article Online
View Journal | View Issue

Cite this: *RSC Adv.*, 2023, **13**, 26247

Development of a novel near-infrared molecule rotator for early diagnosis and visualization of viscosity changes in acute liver injury models†

Manlin Fu, Fenglin He, Zhelu Jiang, Xue Chen, Zhenda Xie* and Jin-Feng Hu*

Received 30th June 2023
Accepted 3rd August 2023

DOI: 10.1039/d3ra04391f

rsc.li/rsc-advances

Acute liver injury leading to acute liver failure can be a life-threatening condition. Therefore, timely and accurate early diagnosis of the onset of acute liver injury *in vivo* is critical. Viscosity is one of the key parameters that can accurately reflect the levels of relevant active analytes at the cellular level. Herein, a novel near-infrared molecule rotator, **DJM**, was designed and synthesized. This probe exhibited a highly sensitive (461-fold from PBS solution to 95% glycerol solution) and selective response to viscosity with a maximum emission wavelength of 760 nm and a Stokes shift of 240 nm. Furthermore, **DJM** has exhibited a remarkable capacity to discern viscosity changes induced by nystatin in viable cells with sensitivity and selectivity and further applied in the zebrafish and mouse model of acute liver injury. Additionally, **DJM** may potentially offer direction for the timely observation and visualization of viscosity in more relevant disease models in the future.

Acute liver injury has been identified as a potential trigger for various intracellular stress responses, including but not limited to metabolic stress, oxidative stress, and endoplasmic reticulum stress.[1] Prolonged exposure to stress may elevate the probability of liver cell injury and death, thereby resulting in liver pathologies such as inflammation and fibrosis.[2,3] Therefore, timely detection of acute liver injury is imperative for comprehensive prevention and treatment, ultimately mitigating the extent of liver damage. Notably, intracellular oxidative stress has been closely linked to acute liver injury. Hence, comprehending the interplay between oxidative stress and the onset and progression of acute liver injury holds significant value for clinical research and therapy.

Viscosity is a pivotal intracellular microenvironmental parameter that contributes significantly to the interaction of intracellular biomolecules, chemical signal transmission, and active metabolite diffusion.[4,5] Deviations from normal viscosity values are strongly associated with numerous cellular malfunctions and the onset of pathologies such as Alzheimer's disease, hypertension, diabetes, and even cancer.[6–8] Recently, it has been reported that viscosity can accurately reflect the level of oxidative stress in the body.[9–11] Consequently, the development of a convenient tool for the precise monitoring of cellular viscosity fluctuations is imperative. In recent years, fluorescence imaging has gained significant attraction due to its real-time visualization, high sensitivity, and relative simplicity of operation.[12,13] Therefore, fluorescence spectroscopy-based detection of intracellular viscosity could potentially emerge as a novel and effective method for the early diagnosis of acute liver injury.

To date, substantial progress has been made in imaging viscosity alterations *in vivo*.[14–20] However, existing probes are not capable of accurately monitoring changes in viscosity within organisms due to their shorter wavelengths or lower sensitivity. In 2023, Li group reported a near-infrared fluorescence probe, designated as **QX-V**. The probe demonstrated a significant increase in fluorescence intensity, by approximately 42.8-fold, in response to changes in viscosity from 1.2 cP to 1023 cP.[21] In 2022, Xu group reported a novel viscosity probe based on dicyanoisophorone, designated as **NV1**. The emission wavelength of probe **NV1** is 590 nm.[22] Henceforth, it is of great significance to fabricate fluorescent probes with superior sensitivity capabilities and near-infrared emission wavelengths, specifically tailored to selectively respond to changes in viscosity within various disease models.[23–25]

Herein, a highly-sensitive near-infrared probe (named **DJM**) was developed by modifying a coumarin derivative as a strong donor as well as the rotor, while dicyanoisophorone acted as an electron acceptor, building upon our prior research (Scheme 1).[26] This probe possesses a remarkably larger Stokes shift (240 nm), and it displays more highly sensitive turn-on signal responses (461-fold at 760 nm) to viscosity. In addition, the probe **DJM** can be applied to detect viscosity in the presence of other interfering ions. Using **DJM** as a chemical tool, we successfully monitored the viscosity variation in Miha cells. Furthermore, the practicability of **DJM** has been further

Institute of Natural Medicine and Health Products, School of Pharmaceutical Sciences, Zhejiang Provincial Key Laboratory of Plant Evolutionary Ecology and Conservation, Taizhou University, Zhejiang 318000, China. E-mail: jfhu@tzc.edu.cn

† Electronic supplementary information (ESI) available. See DOI: https://doi.org/10.1039/d3ra04391f

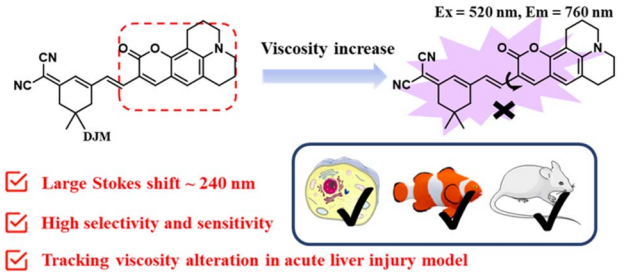

Scheme 1 The structure of probes used in previous work and this work.

confirmed by the acute liver damage model of zebrafish and mouse liver tissues. We believe that **DJM** can provide a convenient and efficient method for more promising clinical applications.

Experimental section

Materials and apparatus

The materials and instruments used in the work could be found in the ESI.†

Synthesis of DJM

The synthetic route of probe **DJM** shows in Scheme S1,† the final steps are as follows: compound **1** and compound **2** were synthesized according to the previous methods.[26,27] The detailed information of instruments used in this work were provided in ESI.†

Compound **1** (22.4 mg, 1.2 mmol), compound **2** (26.9 mg, 1 mmol) and EtOH (5 mL) refluxed for 6 h at 80 °C in a 25 mL round bottomed flask with a few drops of piperidine. After cooling to room temperature, the solvent was removed under reduced pressure. Then, the crude product was purified by column chromatography using CH_2Cl_2/MeOH (v/v = 10 : 1) to obtain **DJM**, a purple solid (26.2 mg, yield 60%). ^{1}H NMR (400 MHz, $CDCl_3$): δ 7.69 (s, 1H), 7.16 (d, J = 6.8 Hz, 2H), 6.90 (s, 1H), 6.79 (s, 1H), 3.34 (q, J = 5.7 Hz, 4H), 2.89 (t, J = 6.3 Hz, 2H), 2.78 (t, J = 6.2 Hz, 2H), 2.56 (s, 2H), 2.46 (s, 2H), 1.98 (p, J = 6.1 Hz, 5H), 1.06 (s, 6H). ^{13}C NMR (100 MHz, $CDCl_3$): δ 169.24, 161.44, 154.80, 151.47, 147.21, 140.46, 132.13, 128.53, 125.94, 122.90, 119.38, 114.57, 113.11, 108.91, 106.22, 50.25, 49.84, 43.01, 39.09, 32.02, 28.02, 27.50, 21.26, 20.30, 20.19. LR-ESIMS: m/z 460.20 ($C_{28}H_{27}N_3O_2$, $[M + Na]^+$).

Monitoring viscosity in mouse model of acute liver injury

Prior to the start of the experiments, mice were acclimated for 7 days after arrival. All study groups contained n = 3 mice. After overnight fasting, the mice were intraperitoneally injected with APAP (300 mg kg^{-1}, 200 μL) to establish an acute liver injury model. Mice in the control group were pretreated intraperitoneally with 200 μL PBS for 2 h. All animal procedures were performed in accordance with the Guidelines for Care and Use of Laboratory Animals of Taizhou University and approved by the Animal Ethics Committee of Taizhou University. During the experiments, all efforts were made to minimize animal suffering. After direct injection of the probe **DJM** (50 μM, 100 μL) into the livers of the acute liver injury model and control mice. The abdominal cavity was then opened and the liver was removed for fluorescence imaging.

Results and discussion

Design strategy of the probe DJM

The viscosity-sensitive probe generally comprises a fluorophore and a rotor linked *via* a C=C bond, based on the Twisted Intramolecular Charge Transfer (TICT) mechanism.[28–30] In our previous work, we reported a NIR fluorescent probe **DJH** based on the D–π–A structure.[26] However, the relatively short emission wavelength of **DJH** was inadequate for detecting living organisms. To overcome this limitation, we extended the conjugated system to red-shift the fluorescence wavelength. We utilized 9-formyl-8-julolidinol to synthesize a coumarin derivative (Scheme 1). The vinyl group, coupled to the isophorone derivatives *via* σ-bonds, served as a viscosity-sensitive group, enabling **DJM** to indicate viscosity changes. In low-viscosity environments, the unrestricted rotation of the rotor around the C–C bond led to the non-radiative quenching of the excited state. However, an increase in viscosity induced a constraint on the rotor's rotation, which triggered the activation of fluorescence.

The response of DJM to viscosity

As mentioned above, the probe **DJM** has the properties of a molecular rotor as a viscosity-sensitive group. Thus, we studied the spectral properties of **DJM** in water–glycerol mixtures. The absorption maxima of **DJM** (λ_{abs}) is about 520 nm and increases gradually with the addition of glycerol (Fig. S1†). When excited at 520 nm, a fluorescence emission peak (λ_{em}) near 760 nm was observed, which was red-shifted compared to our previous work (675 nm), as depicted in Scheme 1. This could be the reason for the enlarged conjugated structure of the chromophore system favoring electron delocalization. It is worth mentioning that **DJM** shows a remarkable viscosity-dependent effect from water (~0.893 cP) to glycerol (~945 cP). The fluorescence intensity at 760 nm is significantly increased by a factor of ~461-fold (when excited at 520 nm). By plotting the log($I_{760\ nm}$) and log(viscosity) across the range of 1–458 cP (glycerol content 0–80%), as shown in Fig. 1a and b, good linearity can be observed (R^2 = 0.9965). Regarding the fluorescence quantum yield, it was enhanced dramatically by about 386 folds in glycerol (Φ = 0.197) compared to that in water (Φ < 0.001), using Rhodamine B as a reference. This characteristic makes the probe **DJM** highly applicable due to its low background fluorescence. Based on the aforementioned data, **DJM** exhibits a favorable response to changes in viscosity.

Evaluation of the selectivity of DJM towards viscosity

To confirm the specificity of **DJM** as a viscosity detector, we evaluated its response to changes in pH. We added the probe to PBS buffer with varying pH values (resulting in a final pH range of 4.2 to 10.8). Then fluorescence intensity at an emission

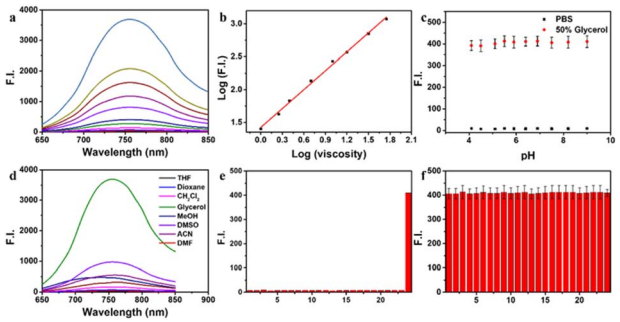

Fig. 1 (a) The fluorescence spectra of probe **DJM** (10 μM) in different ratios of PBS/glycerol mixtures. (b) The linear relationship among log(I_{560}) and log(viscosity) plot in the PBS/glycerol solvents. R^2 = 0.9965. (c) The effect of pH (4.0–9.0) on the relative fluorescence intensity of 10 μM probe **DJM** in PBS solution and PBS/glycerol (v : v = 1 : 1) mixture. (d) The fluorescence spectra of probe **DJM** (10 μM) in different solvents. (e and f) Fluorescence intensity at 760 nm of 10 μM **DJM** toward various species (100 μM) in PBS (e) and PBS/glycerol (v : v = 1 : 1) mixture (f), respectively. (1) Blank; (2) Ser; (3) Phe; (4) Arg; (5) Cys; (6) GSH; (7) Hcy; (8) BSA; (9) SO_3^{2-}; (10) SO_4^{2-}; (11) ClO^-; (12) ClO_4^-; (13) H_2O_2; (14) $ONOO^-$; (15) CO_3^{2-}; (16) OAc^-; (17) NO_3^-; (18) PO_4^{3-}; (19) Cl^-; (20) Fe^{3+}; (21) K^+; (22) Mn^{2+}; (23) Zn^{2+}; (24) 50% glyceral. The excitation wavelength was 520 nm.

wavelength of 670 nm was measured (Ex = 520 nm), as shown in Fig. 1c. The results demonstrate that the fluorescence intensity remained consistent across the entire pH range, indicating that **DJM** is highly resistant to changes in pH and exhibits good photostability.

Evaluating the selectivity of fluorescent probes is crucial to assess their performance, ensuring specificity and avoiding interference from complex cellular components. To this end, we investigated the effect of solvent polarity on the probe **DJM**. We examined the probe's response to various polarities of solvents, including THF, dioxane, DCM, glycerol, MeOH, DMSO, DMF, and ACN. As shown in Fig. 1d, the probe exhibited a much stronger fluorescence intensity in 95% glycerol at 760 nm than in solvents with a small polarity, suggesting that solvent polarity has minimal effect on the fluorescence properties of the probe **DJM**. Furthermore, we measured the fluorescence emission intensity of the probe **DJM** in the presence of high concentrations (100 μM) of interfering ions, disruptors, including biological RSS (Cys, Hcy, GSH, SO_3^{2-}), reactive oxygen species (HOCl, H_2O_2), and various types of anions. As demonstrated in Fig. 1e, the fluorescence intensity of the probe **DJM** in PBS solution in the presence of a high concentration of interfering ions remained almost unchanged compared to that of the pure probe. Remarkably, even in the PBS/glycerol (v : v = 1 : 1) mixture, the probe **DJM** maintained excellent stability towards these ions (Fig. 1f), suggesting that the probe **DJM** can be used to monitor viscosity changes in complex cell environments and has broader applications.

Intracellular fluorescence imaging

First, to assess the biological toxicity of **DJM**, we performed a 2,5-diphenyl-2*H*-tetrazolium bromide (MTT) assay to establish the cytotoxicity test in Miha cells. As shown in Fig. S2,† Miha cells still maintain high viability after incubation with different concentrations of **DJM** (0, 1, 2, 5, 10, 20 μM) for 24 h, indicating that the probe **DJM** has good biocompatibility advantages and is suitable for living cell imaging.

In order to investigate the potential of the probe **DJM** to monitor changes in intracellular viscosity, the ionophore nystatin was used to induce mitochondrial dysfunction and increase intracellular viscosity.[31] Miha cells were divided into two groups: a control group and a nystatin-induced group. As shown in Fig. 2, the control group treated with only the probe **DJM** exhibited weak background fluorescence in the red channel (700–800 nm). In contrast, the fluorescence intensity of the red channel was significantly stronger when cells were cultured with nystatin for 30 minutes and then incubated with the probe **DJM** for another 30 minutes. Furthermore, the mean fluorescence intensity of cell regions (Fig. 2, red channel) was calculated by ROI measurement. The fluorescence intensity in the nystatin-treated cells was 5.4 times higher than that in the non-treated cells. These results clearly indicate that the probe **DJM** is capable of responding to changes in viscosity induced by nystatin in living cells.

Acetaminophen (APAP) is a classical non-steroidal anti-inflammatory drug (NSAID), which is one of the most commonly used antipyretic drugs. At therapeutic doses, APAP is safe and effective, but its excessive use may cause liver damage and result in acute liver failure (ALF). Building on the excellent optical properties of **DJM**, we employed it to detect changes in viscosity in a model of acute liver injury based on Miha cells (Fig. 3). The addition of APAP significantly increased the fluorescence intensity of the cells by approximately three-fold compared to the control group (as per Fig. S3†), indicating an elevation in viscosity when normal liver cells were damaged. We subsequently introduced *N*-acetylcysteine (NAC), a liver-protecting agent that counteracts liver damage caused by APAP. Notably, the fluorescence intensity was significantly reduced to only 1.8-fold that of the control group (Fig. 3c). Collectively, our imaging experiments demonstrate that **DJM** can accurately track viscosity changes in living cells.

Fluorescence imaging in zebrafish model of acute liver injury

In the following study, the application of the **DJM** *in vivo* was further investigated. Zebrafish has been widely used as

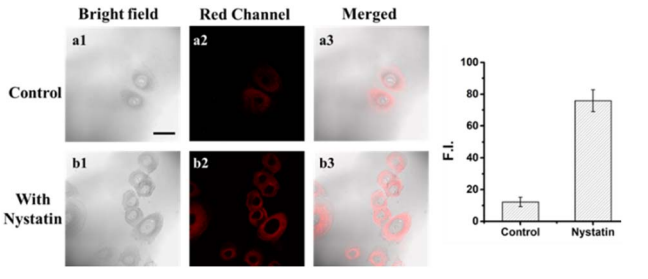

Fig. 2 Imaging of viscosity respectively using Miha cells. (a) As control group, the cells are only dyed with **DJM** (5 μM) for 30 min. (b) The cells were treated with nystatin (10 μM) for 30 min, then dyed with **DJM** (5 μM). (1) bright field; (2) red channel (Ex = 552 nm, Em = 700–800 nm); (3) merged images of (1) and (2). Scale bar: 10 μm.

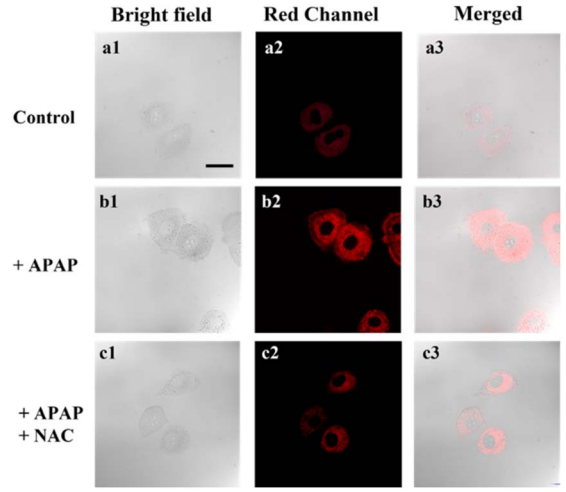

Fig. 3 Fluorescence images of viscosity in Miha cell labeled with **DJM** (10 μM) for 2 h (a) control; (b) after treatment with APAP (200 μM) for 4 h; (c) after treatment with APAP (200 μM) for 4 h, and then treated with NAC (100 μM) for 1 h. (1) Bright field; (2) red channel (Ex = 552 nm, Em = 700–800 nm); (3) merged images of (1), (2). Scale bar: 10 μm.

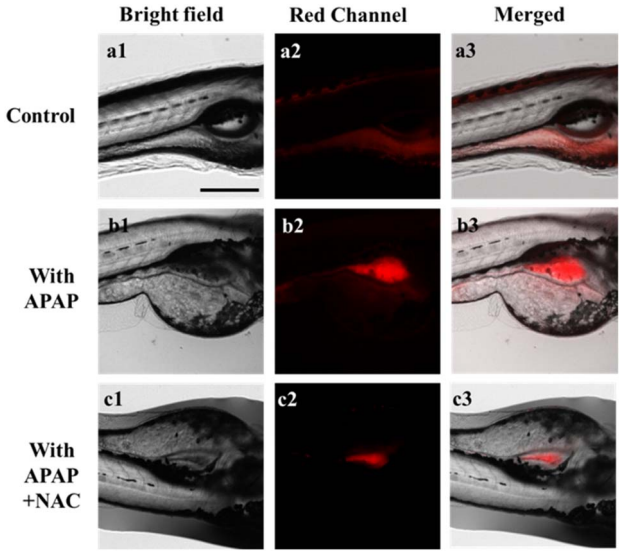

Fig. 4 Fluorescence images of viscosity in living 3 day-old zebrafish. (a) Only labeled with **DJM** (10 μM) for 2 h. (b) After treatment with APAP (200 μM) for 4 h. (c) After treatment with APAP (200 μM) for 4 h, and then treated with NAC (100 μM) for 1 h. (1) Bright field; (2) red channel (Ex = 552 nm, Em = 700–800 nm); (3) merged images of (1), (2). Scale bar: 200 μm.

a biological model due to its strong optical transparency, fast growth, and high genetic similarity to humans.[32,33] To test the ability of **DJM** to detect viscosity changes during liver injury, 3 day-old zebrafish were treated with probe **DJM** (10 μM) for 15 min. In the control group, weak red fluorescence was observed. However, in zebrafish treated with APAP (lipopolysaccharide, an inflammatory stimulator, 200 μM), the fluorescence intensity was significantly higher, indicating an increase in viscosity due to liver injury caused by APAP (Fig. 4b). The fluorescence quantification diagram (Fig. S4†) further revealed that the fluorescence intensity was approximately 4 times higher in the presence of APAP. Conversely, treatment with NAC significantly reduced the fluorescence intensity, with only a 1.6-fold increase compared to the control group (Fig. S4†). These results corroborate those obtained from living cells and provide evidence that **DJM** can be employed to image viscosity changes in zebrafish.

Intracellular fluorescence imaging in mouse model of acute liver injury

Inspired by the promising results obtained in previous experiments, we further assessed the capability of **DJM** to detect viscosity changes in mice. To this end, an acute liver injury model was induced in mice through intraperitoneal injection of APAP, while PBS was used as the control group.[28,29] H&E staining showed significant hepatocyte swelling in the APAP-treated mice, whereas the liver tissues of PBS-treated control mice appeared aligned (Fig. 5a). Fig. 5b demonstrates that the fluorescence intensity of the APAP group was lower than that of the PBS-treated mice (control group). However, the fluorescence intensity of the APAP-treated group was markedly increased upon adding the **DJM** probe, indicating a higher liver viscosity and more severe liver damage in the APAP model group. The experimental results demonstrate that **DJM** can effectively

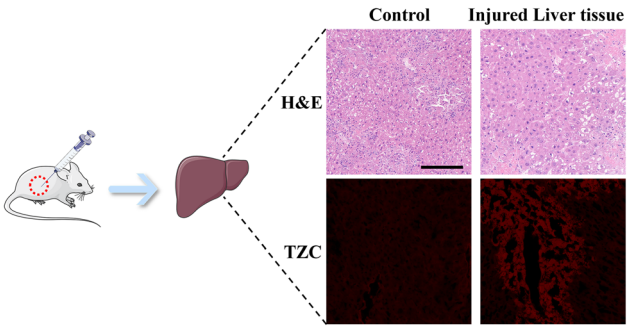

Fig. 5 Schematic diagram of normal and APAP-induced liver tissue in mice and fluorescence imaging of viscosity alteration. Histological study and confocal imaging of liver tissue from APAP-induced liver tissue (300 mg kg^{-1}, 200 μL, 2 h) and PBS (200 μL, 2 h). Scale bar: 100 μm. Red channel (Ex = 552 nm, Em = 700–800 nm). Scale bar: 100 μm.

detect viscosity in the imaging of the mouse liver injury model. Furthermore, the high sensitivity of **DJM** enables the acquisition of clear and accurate fluorescence images, which has significant implications for early diagnosis.

Conclusion

In this paper, a novel NIR viscosity fluorescent probe **DJM** was successfully designed and synthesized. The probe displayed strong fluorescence enhancement at 760 nm with a large Stokes shift (240 nm). Notably, **DJM** exhibited high sensitivity with a 461-fold increment and fine specificity for viscosity in the presence of other analytes. Utilizing **DJM**, we have demonstrated, for the first time, enhanced viscosity levels in acute liver

injury models of live cells, zebrafish, and mice tissues. These findings highlight the effectiveness of constructing a NIR viscosity-sensitive rotor and offer a promising direction for developing new diagnostic methods for viscosity-related diseases.

Author contributions

Manlin Fu: design and synthesis of the probe; Fenglin He: writing – original draft; Zhelu Jiang: data curation; Xue Chen: cell imaging assay; Zhenda Xie: synthesis; Jin-Feng Hu: supervision.

Conflicts of interest

The authors declare no competing financial interest.

Acknowledgements

This work was financially supported by the Natural Science Foundation of Zhejiang Province (LY23H300001) and the National Natural Science Foundation of China (No. 21937002).

References

1 A. Ramachandran and H. Jaeschke, *Curr. Opin. Toxicol.*, 2018, **7**, 17–21.
2 R. Jalan, P. Gines, J. C. Olson, R. P. Mookerjee, R. Moreau, G. Garcia-Tsao, V. Arroyo and P. S. Kamath, *J. Hepatol.*, 2012, **57**, 1336–1348.
3 P. Angeli, P. Gines, F. Wong, M. Bernardi, T. D. Boyer, A. Gerbes, R. Moreau, R. Jalan, S. K. Sarin, S. Piano, K. Moore, S. S. Lee, F. Durand, F. Salerno, P. Caraceni, W. R. Kim, V. Arroyo, G. Garcia-Tsao and A. International Club of, *Gut*, 2015, **64**, 531–537.
4 G. C. Berry, *J. Rheol.*, 1996, **40**, 1129–1154.
5 Y. He, B. X. Wang, L. K. Wen, F. Z. Wang, H. S. Yu, D. X. Chen, X. Su and C. Zhang, *Food Sci. Hum. Wellness*, 2022, **11**, 1–10.
6 Z. Wen, J. Xie, Z. Guan, D. Sun, W. Yao, K. Chen, Z. Y. Yan and Q. Mu, *Clin. Hemorheol. Microcirc.*, 2000, **22**, 261–266.
7 M. R. Fedde and R. F. Wideman Jr, *Poult. Sci.*, 1996, **75**, 1261–1267.
8 G. Sloop, R. E. Holsworth Jr, J. J. Weidman and J. A. St Cyr, *Ther. Adv. Cardiovasc. Dis.*, 2015, **9**, 19–25.
9 A. Kasperczyk, L. Słowińska-Łożyńska, M. Dobrakowski, J. Zalejska-Fiolka and S. Kasperczyk, *Clin. Hemorheol. Microcirc.*, 2014, **56**, 187–195.
10 P. Gyawali, R. S. Richards, E. U. Nwose and P. T. Bwititi, *Clin. Lipidol.*, 2017, **7**, 709–719.
11 D. Konukoglu, M. Ercan and H. Hatemi, *Clin. Hemorheol. Microcirc.*, 2002, **27**, 107–113.
12 M. Fu, Y. Sun, Kenry, M. Zhang, H. Zhou, W. Shen, Y. Hu and Q. Zhu, *Chem. Commun.*, 2021, **57**, 3508–3511.
13 W. Shen, P. Wang, Z. Xie, H. Zhou, Y. Hu, M. Fu and Q. Zhu, *Talanta*, 2021, **234**, 122621.
14 S. Wang, W. X. Ren, J. T. Hou, M. Won, J. An, X. Chen, J. Shu and J. S. Kim, *Chem. Soc. Rev.*, 2021, **50**, 8887–8902.
15 Z. Yang, J. Cao, Y. He, J. H. Yang, T. Kim, X. Peng and J. S. Kim, *Chem. Soc. Rev.*, 2014, **43**, 4563–4601.
16 Y. Q. Lai, Z. D. Xie, M. L. Fu, X. Chen, Q. Zhou and J. F. Hu, *Prog. Chem.*, 2022, **34**, 2024–2034.
17 M. Fu, K. Wang, Q. Ma, J. Zhu, M. Bian and Q. Zhu, *Org. Biomol. Chem.*, 2022, **20**, 672–677.
18 M. Fu, K. Wang, J. Xue, Y. Li, M. Bian and Q. Zhu, *Org. Biomol. Chem.*, 2022, **20**, 3359–3364.
19 G. Q. Fu, Q. T. Liao, Z. Q. Wang, Z. K. Tan, G. J. Mao, B. Yang and C. Y. Li, *Anal. Chim. Acta*, 2022, **1226**, 340192.
20 Y. Wang, S. Li, X. Zhu, X. Shi, X. Liu and H. Zhang, *Anal. Chim. Acta*, 2022, **1202**, 339670.
21 J. J. Chao, H. Zhang, Z. Q. Wang, Q. R. Liu, G. J. Mao, D. H. Chen and C. Y. Li, *Anal. Chim. Acta*, 2023, **1242**, 340813.
22 X. Pan, C. Wang, C. Zhao, T. Cheng, A. Zheng, Y. Cao and K. Xu, *Chem. Commun.*, 2022, **58**, 4663–4666.
23 C. Chen, R. Tian, Y. Zeng, C. Chu and G. Liu, *Bioconjugate Chem.*, 2020, **31**, 276–292.
24 Z. Guo, S. Park, J. Yoon and I. Shin, *Chem. Soc. Rev.*, 2014, **43**, 16–29.
25 C. X. Yan, Y. T. Zhang and Z. Q. Guo, *Coord. Chem. Rev.*, 2021, **427**, 213556.
26 M. Fu, W. Shen, Y. Chen, W. Yi, C. Cai, L. Zhu and Q. Zhu, *J. Mater. Chem. B*, 2020, **8**, 1310–1315.
27 J. Li, L. Tu, Q. Ouyang, S. G. Yang, X. Liu, Q. Zhai, Y. Sun, J. Yoon and H. Teng, *J. Mater. Chem. B*, 2022, **10**, 1427–1433.
28 C. Ma, W. Sun, L. Xu, Y. Qian, J. Dai, G. Zhong, Y. Hou, J. Liu and B. Shen, *J. Mater. Chem. B*, 2020, **8**, 9642–9651.
29 W. Miao, C. Yu, E. Hao and L. Jiao, *Front. Chem.*, 2019, **7**, 825.
30 H. Xiao, P. Li and B. Tang, *Chemistry*, 2021, **27**, 6880–6898.
31 Z. Xie, Y. Zhou, M. Fu, L. Ni, Y. Tong, Y. Yu, N. Li, Z. Yang, Q. Zhu and J. Wang, *Talanta*, 2021, **231**, 122365.
32 A. V. Kalueff, A. M. Stewart and R. Gerlai, *Trends Pharmacol. Sci.*, 2014, **35**, 63–75.
33 Y. J. Dai, Y. F. Jia, N. Chen, W. P. Bian, Q. K. Li, Y. B. Ma, Y. L. Chen and D. S. Pei, *Environ. Toxicol. Chem.*, 2014, **33**, 11–17.